# Is Advection Important? An Examination of the Advective Dynamics of Sensible Heat and Their Influence on Subcanopy Carbon Fluxes in Heterogeneous Terrain

---


By

*Sean Stephen Carrigg*


An Undergraduate Thesis Submitted to
Oregon State University

In partial fulfillment of
the requirements for the
degree of

*Baccalaureate of Science in BioResource Research,*
*Climate and Biosystems Modeling*

August 27th, 2013

APPROVED:

Christoph Thomas, Atmospheric Sciences — Date

Chad Higgins, Biological and Ecological Engineering — Date

Katharine G. Field, BRR Director — Date



Sean S. Carrigg — Date

**Boundary-Layer Meteorology manuscript No.**
(will be inserted by the editor)

# Is Advection Important? An Examination of the Advective Dynamics of Sensible Heat and their Influence on Subcanopy Carbon Fluxes in Heterogeneous Forest Terrain

**Sean S. Carrigg, Christoph K. Thomas**

Received: / Accepted:

**Abstract** Understanding small-scale bio-atmospheric interactions is becoming increasingly important as the global climate continues to change at breakneck speed. A theoretical model of the sensible heat budget of a forest is developed combining conservation equations and concepts from fluid dynamics. Budget components are computationally evaluated using micrometeorological data taken during the period 27 August 2008 - 31 December 2009 within a mature Douglas fir (*Pseudotsuga menziesii*) forest site in the Coast Range of western Oregon, USA. The role of advection in the transfer of sensible heat is explored in the context of the surface energy balance and under conditions of varying turbulence strength. Horizontal variability of wind and temperature is analyzed following methods of Thomas (2011) to re-evaluate the common physical assumptions horizontal homogeneity, uniform gradients, and zero advection. Scalar similarity between sensible heat advection and advective carbon loss in the subcanopy due to vertical decoupling is explored under strong and weak advection conditions using concepts from Thomas et al (2013) and Thomas et al

Bioresource Research
College of Oceanic and Atmospheric Sciences
College of Agricultural Sciences
Oregon State University
Tel.: +1 541 602 2641
E-mail: carriggs@onid.orst.edu, sclerenchyma213@gmail.com

| | Above-Canopy | | Subcanopy | |
|---|---|---|---|---|
| | $k$ $(J\ kg^{-1})$ | $\sigma_w$ $(m\ s^{-1})$ | $k$ $(J\ kg^{-1})$ | $\sigma_w$ $(m\ s^{-1})$ |
| Horizontal | $0.60 < k < 2.8$ | $0.60 < \sigma_w < 1.0$ | $0.10 < k < \mathit{0.70}$ | $0.10 < \sigma_w < \mathit{0.30}$ |
| Vertical | $0.80 < k < 2.1$ | $0.55 < \sigma_w < 0.95$ | $0.05 < k < 0.21$ | $0.07 < \sigma_w < 0.14$ |

**Table 1** Approximate boundaries of TKE ($k$) and $\sigma_w$ corresponding to regions of strong advection in the horizontal and vertical directions, determined from median-binned plots of advection vs. turbulence strength in above-canopy and subcanopy regions. Italicized boundaries correspond to upper bounds of data and not necessarily to upper bounds of regions where advection is strongest.

(2008). It was concluded that (1) advection plays a significant role in energy balance closure at nighttime when turbulent fluxes are small; (2) in general, total advection is non-zero (advective fluxes do not balance out); (3) it is invalid to assume horizontal homogeneity and uniform gradients in heterogeneous terrain; (4) advection tends to be greatest at intermediate values of turbulence strength (TKE or $\sigma_w$); and (5) there is a potential nonlinear relationship between advective carbon loss and sensible heat advection, particularly strong, horizontal advection. Approximate boundaries of turbulence strength corresponding to regions of strong advection are shown in Table 1. Conclusion (5) provides the potential for analyzing biological carbon fluxes using purely physical variables and will be an interesting and necessary topic of future studies.

**Keywords** Advection · Energy balance · Sensible heat · Spatial Variability · Heterogeneity · Subcanopy respiration · Advective carbon loss · Scalar similarity

## 1 Introduction

The global climate is changing at an alarming pace, accompanied by untold environmental damage on all levels of the biological hierarchy ranging from species extinction to the depletion of entire ecosystems. It has become extremely clear during the past several decades that the primary underlying influences of climate change are anthropogenic (human-caused), and this calls for a serious re-evaluation of the place of humanity on this blue planet. The world we once took for granted and saw as nearly infinite in scope is much more fragile than once thought, and it is our duty to treat the earth with a respect on the level of our own lungs, heart and brain. It is our only hope for survival as a species. Our incentive to explore atmospheric processes on all spatial scales is greater than ever, and yet our understanding of meteorological phenomena is largely limited to large-scale climatological studies which provide little information regarding the direct effects of atmospheric change on living things. To truly gain a grasp of bio-atmospheric interactions, much more emphasis must be placed on small-scale meteorology (micrometeorology) in the context of specific ecological terrain. In the present study, we examine the role of advective heat transfer occurring within a Douglas fir (*Pseudotsuga menziesii*) forest in the hope of better understanding how heat and energy are transported within heterogeneous biotic terrain. We also examine the influence of heat advection on carbon fluxes within the forest site to determine whether sensible heat advection can be an effective predictor of advective carbon loss in the subcanopy resulting from vertical decoupling.

## 1.1 The Surface Energy Balance

The surface energy balance is a fundamental principle arising from the laws of mass and energy conservation which forms the basis for the description of a wide array of micrometeorological phenomena. The energy balance concept states that the net radiation $R_N$ at the surface of the earth must be equal in magnitude to the sum of all heat fluxes which occur within the atmospheric boundary layer when the surface and boundary layer are in equilibrium with one another (Foken, 2008a). In other words, the net sum of all convective heat transfer and storage processes occurring at or near the surface of the earth are driven by the available energy from all solar and terrestrial radiative fluxes. The available energy is redistributed as sensible ($H$) and latent ($\lambda E$) heat (Arya, 2001), where $\lambda$ is the latent heat of vaporization of water and $E$ is the rate of evapotranspiration. Both sensible and latent heat play immense roles in the characterization of atmosphere-vegetation interactions and the energy dynamics of micrometeorological systems. The component of the net radiation which does not contribute to sensible or latent heating is conducted by the ground surface as the soil heat flux $G$ (Stull, 1988). The basic surface energy balance equation can be expressed as follows,

$$-(R_N + G) = H + \lambda E \tag{1}$$

where the left-hand side of Equation 1 represents the net available energy for the transfer of sensible and latent heat. The negative sign on the available energy is the result of the convention that all energy fluxes directed away from the earth's surface are positive, and all fluxes directed toward the surface are negative (Foken, 2008a). Sensible and latent heat can be separated into individual budget equations which describe the various modes of energy transfer. There are three primary modes of transfer involved in the transport of energy within the boundary layer, including advection, turbulence, and storage; few studies have been devoted to the experimental evaluation of all such components (e.g., Moderow et al, 2007). We will explore the behavior of each mode of energy transfer within the context of the energy balance of a Pacific Northwest forest ecosystem comprised primarily of mesic Douglas fir (*Pseudotsugas menziesii*). We are primarily interested in the role of sensible heat advection in energy transport.

## 1.2 Radiative Transfer

Radiative transfer is a separate topic on its own, but an understanding of energy transfer via radiation is essential for one to be able to comprehend the meaning and significance of the surface energy balance. Here we present a brief conceptual description of the various constituents of the radiation budget. The radiation budget consists of both shortwave ($0.15 < \lambda < 3\ \mu m$) and longwave ($3 < \lambda < 100\ \mu m$) radiation components which occur in reference to a horizontal plane and are the result of the direct emission of solar and terrestrial radiation, absorption/re-emission by the atmosphere, and scattering (Arya, 2001). In other words, the net radiation is equal to the sum of upwelling ($\uparrow$) and downwelling ($\downarrow$) longwave ($I$) and shortwave ($K$) radiation components (Stull, 1988):

$$R_N = K\downarrow + K\uparrow + I\downarrow + I\uparrow \tag{2}$$

There are a variety of methods for measuring net radiation, each with its own limitations (Halldin and Lindroth, 1992; Vogt and Thomas, 1995). Accurately and precisely measuring the net radiation in will be an important factor in determining the degree of energy balance closure (i.e., the size of the difference between the net radiation and the sum of all experimentally evaluated heat fluxes).

## 1.3 Sensible and Latent Heat Budgets

Sensible heat is energy which contributes to changes in temperature, while latent heat is characterized by the evaporation of water and contributes to changes in humidity (Stull, 1988). Sensible heat and latent heat can be transported via advective processes corresponding to mean flow, turbulent processes corresponding to statistical fluctuations from the mean, and can be stored. Separating mean flow from statistical fluctuations is mathematically defined as Reynolds decomposition (Foken, 2008a) and is an essential step in the development of equations of motion describing heat flow phenomena in the atmosphere. Here we will provide brief descriptions of advection, turbulence, and storage in terms of their physical concepts and mathematical flux operators. We will provide a more quantitative and rigorous mathematical treatment of the corresponding equations of motion in Section 2.

1. **Advection**: A form of convective transport corresponding to the bulk motion of a fluid. Advection is driven by flow velocity and the spatial gradient of

the flow quantity of interest. Mathematical flux operator: $\hat{A} \equiv \mathbf{v} \cdot \nabla$.

2. **Turbulence**: A second form of convective transport corresponding to stochastic fluctuations from mean flow. Turbulent fluxes can be expressed as co-perturbations of wind velocity and the flow quantity of interest. Mathematical flux operator: $\hat{Q} \equiv \nabla \cdot \mathrm{Cov}(\mathbf{v}, \cdot)$.

3. **Storage**: The rate at which a particular flow quantity is stored within a given control volume $\tau$. Storage represents the net gain or loss of a system balanced by fluxes and the net generation due to the presence of sources or sinks. Mathematical flux operator: $\hat{S} \equiv \frac{\partial}{\partial t}$.

## 1.4 Energy Balance Closure

The underlying mechanisms of advection, turbulence, and storage are identical for both sensible and latent heat, while the relative contribution of each energy component on the total energy budget can vary drastically depending on the structure of the ecosystem of interest and the spatiotemporal scales at which the fluxes are measured (Thomas, 2011; Foken et al, 2006; Foken, 2008b). In other words, the magnitude of the total sensible heat flux and the total latent heat flux is strongly dependent on terrain, topography, climate and surface properties. The relative influence of sensible heat to latent heat on the total energy budget is often described in terms of the Bowen Ratio $Bo \equiv \frac{H}{\lambda E}$ (Bowen, 1926). Within our forest site, $Bo > 1$ and therefore sensible heat transfer predominates. Because of this fact, we chose to focus on the evaluation of the terms comprising the sensible heat budget and assume all non-turbulent terms of the latent heat budget to be negligible.

The energy balance concept outlined in the past several sections combining conservation of energy with the convective transport phenomena of advection, turbulence, and storage remains to be the most accurate and reliable quantitative description of energy transfer within the atmospheric boundary layer. However, many shortcomings exist based on underlying theoretical assumptions and experimental techniques which lead to inconsistencies between observed energy fluxes and the net available energy. The degree of energy balance closure is most commonly expressed in terms of the *residual* $R$, defined as the difference between the net radiation and sum of all heat fluxes. Although conservation of energy dictates that the surface energy budget must be closed ($R = 0$), the vast majority of experimental studies of the surface energy budget have failed to confirm this fact (e.g., Leuning et al, 2012). In most cases, the sum of energy fluxes has been found to be less than that of the net available energy ($R > 0$); it is not uncommon to observe only 80 percent closure of the total energy budget (Anthoni et al, 2000; Foken, 2008b). The problem of energy balance closure has been at the forefront of micrometeorological research in recent decades, and much effort has gone into improving understanding of the nature of energy budget closure and determining sources of error and uncertainty (Moderow et al, 2009, 2007; Foken et al, 2006; Thomas, 2011). Due to the chaotic nature of meteorological phenomena, it is quite a challenge to precisely pinpoint the sources of poor energy budget closure. Doing so requires a reassessment of fundamental assumptions regarding the energy budget and evaluation of energy budget components. Here we will discuss some of the most common assumptions which are thought to play a role in the underestimation of the energy budget.

### 1.5 Potential Causes of Poor Budget Closure

The most common assumptions concerning the evaluation of the surface energy budget are due to experimental limitations. Energy budget components depend on spatial gradients which can only be computed using rough linear approximations or spatial averaging techniques because of sparse station networks. Often horizontal homogeneity is assumed, corresponding to zero variability in the horizontal domain; this reduces evaluation of the surface energy budget to a one dimensional problem by assuming fluxes only occur in the vertical direction. However, such assumptions are typically too stringent, as the vast majority of micrometeorological systems harbor some degree of horizontal variability (Thomas, 2011). If horizontal variation is taken into account, it is common to assume uniform horizontal gradients. The accuracy of this assumption strongly depends on the system of interest (e.g., topography and complexity of terrain) as well as spatiotemporal scale. Other common assumptions include zero mean vertical wind speed (corresponding to zero vertical advection) or the claim that the horizontal and vertical advective fluxes "balance out," giving rise to zero total advection. Several previous studies indicate that neglecting the influence of advective flow can result in the underestimation of net energy fluxes, especially at night when advective forces dominate due to stable stratification (Moderow et al, 2009, 2007). Analogous studies have been conducted concerning the advection of carbon dioxide with respect to the carbon mass balance (Aubinet et al, 2010, 2005). Other research indicates that errors in the estimation of turbulent fluxes (e.g., incorrect determination of temporal and spatial scales) may also play a role (Foken et al, 2006; Foken, 2008b).

## 1.6 Advective Carbon Loss and the Carbon Mass Balance

Sensible heat advection may influence the carbon mass balance in addition to the energy balance. Changes in atmospheric carbon dioxide concentrations have the most immediate effects on climate change and ecological systems due to the tight coupling of carbon dioxide with biological processes. Carbon dioxide remains to be the optimum variable for analyzing bio-atmospheric interactions. However, the dynamics of carbon dioxide in an ecosystem must include analysis of the complex metabolic processes which give rise to carbon uptake and release (i.e., photosynthesis and respiration, respectively) in addition to the atmospheric dynamics of carbon dioxide. The uncertainty of the net effects of such processes in a given ecosystem make the carbon mass balance (analogous to the energy balance) difficult to analyze. Therefore, understanding the relationship between heat advection and carbon dioxide transport is an important consideration. In a study by Thomas et al (2013), advective loss of carbon dioxide released via subcanopy respiration was shown to be a possible cause for the underestimation of NEE (net ecosystem exchange) as a result of decoupling between the above-canopy layer and the subcanopy and ground surface layers. If a relationship between sensible heat advection and advective carbon loss in the subcanopy resulting from such decoupling exists, a simpler method for determining the degree of carbon loss may be developed which uses a purely physical quantity to describe a complex biological process.

## 1.7 Experimental Objectives

This study was completed with the intention of improving understanding of the underlying mechanisms of energy transfer in forest ecosystems. The primary objectives of the present study were to (i) develop a theoretical model of the generalized heat budget as a means for computing energy budget components and compare various calculation options (i.e., spatial averaging vs. linear approximation), (ii) evaluate the validity of the common physical assumptions of horizontal homogeneity, uniform gradients and zero advection in heterogeneous terrain, (iii) investigate the role of advection in the transfer of sensible heat in the context of the total surface energy balance and under various physical conditions, and (iv) explore scalar similarity between sensible heat advection and carbon fluxes to determine whether sensible heat advection is an effective predictor of advective carbon loss.

# 2 Background Theory

## 2.1 Derivation of the Generalized Heat Budget Equation

Consider the fluid motion of a space- and time-dependent transport quantity $\phi(\mathbf{r},t)$ through a predefined control volume $\tau$ (height $\Delta z$, base area $A$) at velocity $\mathbf{v}(\mathbf{r},t)$. [Fluid velocity is commonly expressed in terms of Cartesian components $(u\ \ v\ \ w)$, which correspond to the East-West, North-South and Up-Down axes, respectively]. By the law of conservation, the rate of storage of $\phi$ in $\tau$ is equal to the net flux plus the net generation due to all sources and sinks:

$$[\textbf{Rate of Storage}] \;=\; [\textbf{Net Flux}] \;+\; [\textbf{Net Generation}] \tag{3}$$

The rate of storage is defined as the (partial) time derivative of the transport quantity $\phi$. The total flux is equal to the sum of all fluxes (expressed as surface integrals) due to flux contributions $\mathbf{J}_i(\mathbf{r},t)$. The net generation due to all sources and sinks is equal to the sum of all sources and sinks $\Gamma_j(\mathbf{r},t)$. Hence, 3 is expressed mathematically as:

$$\frac{\partial \phi(\mathbf{r},t)}{\partial t} \;=\; \sum_i \oint_A \mathbf{J}_i(\mathbf{r},t)\cdot d\mathbf{A} \;+\; \sum_j \Gamma_j(\mathbf{r},t) \tag{4}$$

where the differential area vector $d\mathbf{A} \equiv \hat{\mathbf{n}}\ dA$ and the unit normal vector $\hat{\mathbf{n}}$ points inward from the surface of $\tau$ for convenience. This is the most general form of the *continuity relation* describing the fluid motion of $\phi$ in the control volume $\tau$. Let us define the volume density $\rho(\mathbf{r},t) = \frac{d\phi}{d\tau}$ and the per-unit-volume source strength as $\gamma(\mathbf{r},t) = \frac{d\Gamma}{d\tau}$. According to the Divergence Theorem, $\oint_A \mathbf{J}_i(\mathbf{r},t) = -\int_\tau \nabla\cdot\mathbf{J}_i(\mathbf{r},t)d\tau$. After some substitution and simplification, we obtain the following local, differential form of Equation 4:

$$\frac{\partial \rho(\mathbf{r},t)}{\partial t} \;+\; \sum_i \nabla\cdot\mathbf{J}_i(\mathbf{r},t) \;=\; \sum_j \gamma_j(\mathbf{r},t) \tag{5}$$

If the RHS of Equation 5 $> 0$, $\tau$ is a net *source*. If the RHS of Equation 5 $< 0$, $\tau$ is a net *sink*. If the RHS of Equation 5 = 0, $\tau$ is neither a source nor sink and $\rho$ is a *conserved* quantity (e.g., mass, energy, momentum, charge, etc.). We will be dealing with energy exchanges among the subcanopy and above-canopy layers of forest land cover and will treat the exchange of solar and terrestrial radiation as the primary energy *source* for driving such energy transfer processes. We will be concerned only with convective (i.e., advection and turbulence) and radiative fluxes in the context of the surface energy balance; molecular diffusive processes $(\mathbf{J}_D \equiv -D\nabla\rho)$ in the atmosphere generally make a negligible contribution to energy transfer (Foken, 2008a). The convective flux contribution is defined as $\mathbf{J}_C \equiv \rho\mathbf{v}$, the product of the transport quantity and the flow velocity; the functional notation has been dropped for simplicity. Correspondingly, the source strength term is represented by the radiative flux $\sigma(\mathbf{r},t)$. The magnitude of $\sigma$ is a per-unit-volume source strength because it delineates the degree to which the control volume $\tau$ absorbs radiation from an outside source (in the context of this study, the sun). Equation 5 therefore reduces to:

$$\frac{\partial\rho}{\partial t} + \nabla\cdot\rho\mathbf{v} = \sigma \tag{6}$$

Equation 6 represents the continuity equation for our system and forms the basis for the derivation of the energy budget equation. We must apply Reynolds averaging to Equation 6 to emphasize the independence of mean flow (advection) and statistical fluctuations from the mean (turbulence). Recall Reynolds decomposition of a quantity $x$, where overbars represent time averages and primes represent fluctuations from the average: $x = \overline{x} + x'$. The mean of the product of two Reynolds-decomposed variables $x$ and $y$ yields Reynolds' Second Postulate: $\overline{xy} = \overline{(\overline{x}+x')(\overline{y}+y')} = \overline{x}\ \overline{y} + \overline{x'y'}$ (Foken, 2008a, pp. 26-31). In other words, the mean of the product of two variables is equal to the product of the variable means plus the covariance of the two variables. Application of Reynolds' Second Postulate to Equation 6 and expansion via the product rule yields:

$$\begin{aligned} \overline{\sigma} &= \frac{\partial\overline{\rho}}{\partial t} + \nabla\cdot\overline{\rho\mathbf{v}} \\ &= \frac{\partial\overline{\rho}}{\partial t} + \nabla\cdot\overline{\rho}\ \overline{\mathbf{v}} + \nabla\cdot\overline{\rho'\mathbf{v}'} \\ &= \frac{\partial\overline{\rho}}{\partial t} + \overline{\mathbf{v}}\cdot\ \nabla\overline{\rho} + \overline{\rho}\ \nabla\cdot\overline{\mathbf{v}} + \nabla\cdot\overline{\rho'\mathbf{v}'} \end{aligned} \tag{7}$$

In most cases, the atmosphere is seen as approximately incompressible $(\nabla\cdot\overline{\mathbf{v}} = 0)$ over sufficiently long averaging periods (Moderow et al, 2007); we will adopt this assumption. For further notational simplification, let us adopt the Einstein summation convention (e.g., Feigenwinter et al, 2004; Finnigan, 1999). Equation 7 therefore reduces to:

$$\overline{\sigma}(x_i,t) \;=\; \underset{\text{I.}}{\frac{\partial \overline{\rho}}{\partial t}} \;+\; \underset{\text{II.}}{\overline{u}_i \frac{\partial \overline{\rho}}{\partial x_i}} \;+\; \underset{\text{III.}}{\frac{\partial \overline{u_i' \rho'}}{\partial x_i}} \;=\; \hat{S}\,\overline{\rho} + \hat{A}\,\overline{\rho} + \hat{Q}\,\overline{\rho} \tag{8}$$

Here $x_i$ represents the three Cartesian coordinates ($x$, $y$, and $z$), and $u_i$ represents the corresponding wind velocity components ($u$, $v$, and $w$). Equation 8 represents the combined effects of I. storage, II. advection (bulk flow), and III. turbulence (statistical fluctuations) on the transfer of energy driven by the source injection term $\sigma$. Equation 8 can be integrated over $\tau$ and normalized with respect to the base area $A$ to obtain an expression for the generalized flux density $\overline{\xi}(x_i,t)$:

$$\overline{\xi}(x_i,t) \;=\; \int_0^z \langle \frac{\partial \overline{\rho}}{\partial t} \;+\; \overline{u}_i \frac{\partial \overline{\rho}}{\partial x_i} \;+\; \frac{\partial \overline{u_i' \rho'}}{\partial x_i} \rangle \; dz \tag{9}$$

The angled brackets $\langle \cdot \rangle \equiv \frac{1}{A} \int \int_A \; [\cdot]\, dx\; dy$ represent spatial averaging over the horizontal domain. It is commonly assumed that horizontal variation corresponds to horizontal components of the energy budget and vertical variation corresponds to vertical components. After separation into horizontal and vertical components, we obtain the complete expression for the generalized flux density $\overline{\xi}(x,y,z,t)$:

$$\begin{aligned} \overline{\xi}(x,y,z,t) \;=\; & \int_0^z \frac{\partial \overline{\rho}}{\partial t}\; dz + \int_0^z \langle \overline{u} \frac{\partial \overline{\rho}}{\partial x} \;+\; \overline{v} \frac{\partial \overline{\rho}}{\partial y} \rangle \; dz + \int_0^z \overline{w} \frac{\partial \overline{\rho}}{\partial z}\; dz \\ & + \int_0^z \langle \frac{\partial \overline{u' \rho'}}{\partial x} \;+\; \frac{\partial \overline{v' \rho'}}{\partial y} \rangle \; dz + \int_0^z \frac{\partial \overline{w' \rho'}}{\partial z}\; dz \end{aligned} \tag{10}$$

The terms on the RHS of Equation 10 represent storage ($S$), horizontal advection ($A_h$), vertical advection ($A_v$), the horizontal flux divergence ($Q_h$) and the vertical turbulent flux ($Q_v$) (respectively). In the context of the sensible heat budget, the energy density $\rho = \rho_a c_p T$ where $\rho_a$ is air density, $c_p$ is the specific heat of moist air at constant pressure, and $T$ is air temperature. In the context of the latent heat budget, the energy density $\rho = \lambda \rho_a q$, where $\lambda$ is the latent heat of vaporization, $\rho_a$ is air density, and $q$ is specific humidity. An analogous equation can be used to describe the carbon budget, where the mass density $\rho = [CO_2]$, the atmospheric concentration of carbon dioxide.

## 3 Data Collection and Analysis

### 3.1 General site description

Wind and temperature data were collected in a 37-year-old mature Douglas fir (*Pseudotsuga menziesii*) forest site located in the Coast Range of western Oregon, USA (AmeriFlux site US-Fir, 44.646$^\circ$ N latitude, 123.551$^\circ$ W longitude, 310 m elevation; see Fig.1; Thomas et al, 2008) over the period of 27 August 2008 to 31 December 2009. The vertical structure of the system consisted of a sparse understory comprised primarily of salal (*Gaultheria shallon*) up to a mean height of 0.8 m. The crown space extended from approximately 15 m to an average canopy height of 28 m. The leaf area index (LAI) of the forest canopy was measured optically in 2004 (Model LAI2000, Licor, Lincoln, Nebraska, USA) to be approximately 9.4 $\mathrm{m}^2\,\mathrm{m}^{-2}$. Results from a study by Thomas (2011) at the same site indicate that such a high LAI leads to a reversed static stability regime in the crown space and subcanopy. The site is surrounded by moderately complex topography, with a flat saddle located approximately 600 m NE of the defined center of the site. The complexity of the topography and terrain serves as a potentially useful tool for exploring the assumption of horizontal homogeneity and negligible advection within heterogeneous landscapes.

### 3.2 Sensor network

The system was comprised of a horizontal array and vertical profile of wind and temperature sensors along with two eddy covariance stations located within the subcanopy and above-canopy regions. A soil thermal probe (Model CS107, Campbell Scientific Inc., Logan, UT, USA) was also used to measure soil temperature at varying depths (2, 4, 8, 16, 32, and 64 cm) with logarithmic spacing, and a net radiometer (Model CNR-1, Kipp and Zonen, Delft, The Netherlands) was mounted above the canopy (38.5 m) to measure the net radiation. Each station comprising the horizontal array and vertical profile consisted of one 2-D sonic anemometer (Model WAS425A, Vaisala Inc., Helsinki, Finland) and one air temperature sensor (external thermistor, Model HOBO H8 Pro, Onset Computer, Bourne, MA, USA) in a naturally ventilated radiation shield (Model M-RSA, Onset Computer, Bourne, MA, USA). The horizontal array consisted of 10 stations (S01 and S04-S12) distributed over a domain extending 180 m (West-East) by 205 m (North-South); all measurement devices were mounted 1 m above ground level on a guyed tripod. Figure 1 diagrams the site and shows the relative coordinates of all horizontal array stations with respect to the defined center of the site. The vertical profile and eddy covariance stations were located

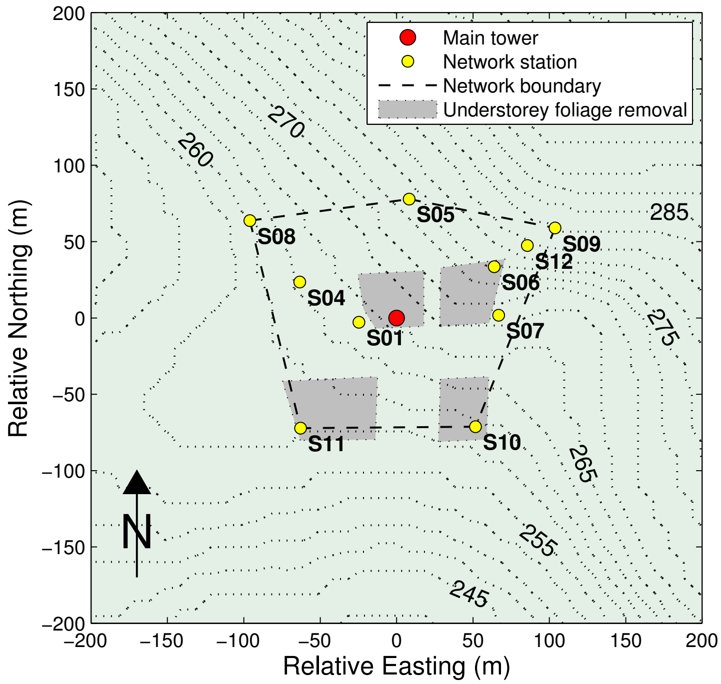


**Fig. 1** Diagram of experimental site. Elevation contours are in meters. Yellow circles represent stations (1 m a.g.l.) comprising horizontal array of wind and temperature sensors. The red circle represents the main tower housing the vertical profile of wind and temperature sensors (0.5, 2.0, 4.5, 9.3, 13.0, 19.0, 26.8, and 37.5 m a.g.l.) as well as the eddy covariance stations (4.0 m and 38.3 m a.g.l.). Adapted from Thomas (2011).

on the main tower at the geographic center of the site. The vertical profile was comprised of 8 stations at varying heights above ground level (0.5, 2.0, 4.5, 9.3, 13.0, 19.0, 26.8, and 37.5 m). The two eddy covariance stations, each consisting of one 3-D sonic anemometer (CSAT3, Campbell Scientific Inc., Logan, UT, USA) for measuring vertical wind speed, one temperature sensor (external thermistor, Model HOBO H8 Pro, Onset Computer, Bourne, MA, USA), and an infrared $H_2O$ and $CO_2$ gas analyzer (Model Li-7500/7000, Licor Environmental, Lincoln, NE, USA), were respectively located at 4.0 m and 38.3 m above ground level.

All sonic anemometers comprising the horizontal array and vertical profile internally sampled horizontal wind speed and direction at a frequency of 1 Hz and all data was stored in a central data logger (Model CR5000, Campbell Scientific Inc., Logan, UT, USA) at a 10 s running average using serial digital interface (SDI) communication among the entire network. Air temperature measurements were sampled and stored every 2 minutes on the onboard data logger of each sensor; the large sampling interval is due to the large time constant of the thermistor ($\tau_{thermistor}$ = 122 $\pm$ 6 s, Whiteman et al (2000)). Instruments were calibrated according to the methods of Thomas (2011).

All wind and temperature data were aggregated to 20 minute block averages prior to processing. This was deemed to be within the appropriate time scale range for turbulence analysis, which typically ranges from 20 to 30 minute intervals at the spatial scale of our system. The time interval cannot be arbitrarily chosen, as net energy balance closure has been shown to be highly dependent on time scale with the use of ogive function statistics, i.e. the converging frequency of the cumulative turbulence co-spectrum (Foken et al, 2006). Smaller or larger time intervals would likely lead to loss of information and thus poor closure; Vickers et al (2009) addresses this issue in the context of the carbon mass balance. Nonetheless, the goal of this study is not to close the energy budget, but to investigate the influence of sensible heat advection on the energy and carbon mass balances under a variety of physical conditions.

### 3.3 Computational Methods

The equations derived in Sections 1 and 2, particularly that of Equation 10, were used to individually compute the components of the sensible heat budget which were assumed to dominate (i.e., vertical turbulence, horizontal advection, vertical advection, and storage). The horizontal flux divergence was assumed to be zero, a claim which has been justified by several studies; e.g., Moderow et al (2007) determined that the horizontal flux divergence has the lowest mean value of all energy flux components in tall plant canopies. Following directly from Equation 10, all sensible budget terms can be computed using experimental wind and temperature measurements. The vertical latent turbulent flux was also included in the total energy budget using specific humidity measurements obtained from the gas analyzers, but all other terms of the latent heat budget were neglected due to the fact that $Bo > 1$ throughout the majority of the day. The following paragraphs describe the computational methods used to evaluate each term in Equation 10 in the context of the sensible heat budget, recognizing that finite-difference techniques are necessary for analysis of real, discrete data sets. Computational methods for evaluating the carbon budget (e.g., NEE and $R_{SUB}$) are described in detail in Thomas et al (2013) and Thomas et al (2008). Unphysical outliers in data were removed (despiked) by removing upper and lower 0.5-percentiles of budget data prior to analysis.

### 3.3.1 Vertical Turbulent Flux

In the context of the sensible heat budget, total (horizontal and vertical) turbulence is defined as the divergence of the covariance of wind velocity and air temperature integrated over the control volume of interest. [Recall that the covariance of two variables is equivalent to the mean product of the deviations of each variable from their respective means; e.g., $Cov(x,y) = \overline{x'y'} = \overline{(x-\overline{x})(y-\overline{y})}$]. If zero horizontal variability of the vertical turbulent flux is assumed, the sensible vertical turbulent flux is simply the covariance of vertical wind speed and temperature, following the last term of Equation 10. Note that the heat flux coefficient $c_H = \rho_a c_p$ has been included to convert from kinematic to energetic units using averaged measurements from both eddy covariance stations, as it will be used for the computation of all fluxes.

$$Q_{v,H}(t) = c_H \overline{w'T'} \tag{11}$$

The latent vertical turbulent flux $Q_{v,\lambda E}$ can also be computed using Equation 11, substituting the specific humidity $q$ for air temperature and $c_{\lambda E} = \rho_a \lambda$ for the heat flux coefficient.

### 3.3.2 Horizontal Advection

Horizontal advection is the mean flow of a fluid along the horizontal domain, corresponding to the dot product of the horizontal wind velocity components $\overline{u}$ and $\overline{v}$ and the horizontal temperature gradient. To re-evaluate the assumption of horizontal homogeneity within heterogeneous terrain, we chose to compute horizontal advection using two methods: (1) the conventional 3-point gradient (linear approximation) method, where a single temperature gradient is computed using measurements from the three stations determined to be best representative of the entire system; and (2) the spatial averaging method, where a weighted average of temperature gradients corresponding to all possible 3-point subdomains within the 10-station array is applied. While the 3-point gradient method is likely to be inadequate, it was included for the sake of comparison. Each method is described in detail below. The influence of each method on the residual of the energy balance was explored.

*3-Point Gradient Method:* The 3-point gradient method involved the selection of the three stations thought to be most representative of the entire system (Stations S04, S09, and S10). Factors taken into account in the selection of the three stations include the area spanned by the stations, the variation in topography and terrain among the three stations relative to true topography and land cover distribution, wind speed variability, and the similarity of temperature gradients to the spatially averaged gradient. [Note that other station combinations are possible for analysis which also accurately represent the system, but only one combination was included to eliminate redundancy]. The temperature gradient was defined as the gradient corresponding to the plane defined by the space-temperature coordinates of the three stations calculated over the entire time series. The decomposed components $\gamma$ and $\delta$ (corresponding to the East-West and North-South cartesian axes, respectively) of the horizontal temperature gradient are defined as follows in terms of a plane of the form $a_1 \cdot x + a_2 \cdot y + a_3 \cdot T = a_4$:

$$\begin{aligned} \gamma &= \frac{\langle \partial \overline{T} \rangle}{\partial x} = -\frac{a_1}{a_3} \\ \delta &= \frac{\langle \partial \overline{T} \rangle}{\partial y} = -\frac{a_2}{a_3} \end{aligned} \tag{12}$$

The local horizontal advection $a_{h,3p}$ was computed by taking the dot product of the gradient components with the 3-point average wind velocity components $\langle u \rangle$ and $\langle v \rangle$:

$$a_{h,3p} = \gamma \cdot \langle u \rangle + \delta \cdot \langle v \rangle \tag{13}$$

The local horizontal advection can be integrated over the height $\Delta z$ of the system to obtain the total horizontal advection in terms of the 3-point method. Recall that we are assuming zero vertical variability of horizontally varying quantities, just as we are assuming zero horizontal variability of vertically varying quantities. Therefore, the local horizontal advection $a_{h,3p}$ can be treated as constant and we obtain the following expression:

$$A_{h,3p}(t) \; = \; c_H \cdot a_{h,3p} \cdot \Delta z = c_H \cdot [\gamma \cdot \langle u \rangle + \delta \cdot \langle v \rangle] \cdot \Delta z \tag{14}$$

*Spatial Averaging Method:* Our system consists of 10 stations. Therefore, there are a total of $10!/3!7! = 120$ possible triplet subdomains from which a plane can be defined. Let us define the arbitrary subdomain $ijk$ as $s_{ijk}$. In a similar manner to the 3-point method, the gradient of the plane corresponding to $s_{ijk}$ was computed over the entire time series and decomposed into cartesian components $\gamma_{ijk}$ and $\delta_{ijk}$.

The dot product of the subdomain-defined gradient was taken with the corresponding subdomain-averaged wind velocity components (i.e., $\langle u_{ijk}\rangle$ and $\langle v_{ijk}\rangle$) to obtain the local horizontal advection $a_{h,ijk}$ corresponding to subdomain $s_{ijk}$ (equivalent to Equation 13 but defined by subdomain). Given that the area of each subdomain varies, the influence of each subdomain on total advection will vary. Therefore, a weighted average of the computed advection $a_{h,ijk}$ was necessary. The local advection $a_{h,SA}$ for our system can be defined as follows:

$$a_{h,SA} \;=\; \frac{1}{\alpha}\sum_{ijk} A_{ijk}\cdot a_{h,ijk} \qquad (15)$$

where $A_{ijk}$ is the area of subdomain $s_{ijk}$ and $\alpha$ is the sum total area of all subdomains. Finally, the local horizontal advection can be integrated over the height $\Delta z$ of the system to obtain the total horizontal advection. Again, our assumption of zero vertical variability of horizontally varying quantities allows us to treat $a_{h,SA}$ as a constant. We therefore obtain an expression for total horizontal advection:

$$A_{h,SA}(t) \;=\; c_H\cdot a_{h,SA}\cdot\Delta z \;=\; \frac{c_H\cdot\Delta z}{\alpha}\sum_{ijk} A_{ijk}\cdot[\gamma_{ijk}\cdot\langle u_{ijk}\rangle+\delta_{ijk}\cdot\langle v_{ijk}\rangle] \qquad (16)$$

### *3.3.3 Vertical Advection*

Vertical advection is the mean bulk flow of a fluid along the vertical axis, corresponding to the product of vertical wind speed ($\overline{w}$) and the vertical temperature gradient. Vertical advection was computed using two methods analogous to the methods used for computing horizontal advection: (1) the 2-point gradient (linear approximation) method, where measurements from top and bottom stations were used to compute a single temperature gradient; and (2) spatial averaging according to the methods of Lee (1998). While the 2-point gradient method is likely to be inadequate (as is the 3-point gradient method for computing horizontal advection), it was included for the sake of comparison. Each method is described in detail below. As with horizontal advection, the influence of each method on the residual of the energy balance was explored.

*2-Point Gradient Method:* The 2-point gradient method for computing vertical advection is fairly straightforward, involving only the top and bottom stations in the vertical profile. The vertical temperature gradient $\beta$ can be approximated by taking the slope of the line intersecting the space-temperature coordinates corresponding to both stations over the entire time series. For a line of the form $b_1\cdot z+b_2\cdot T=b_3$, $\beta$

is defined as follows:

$$\beta \;=\; \frac{\langle \partial \overline{T} \rangle}{\partial z} \;=\; -\frac{b_1}{b_2} \tag{17}$$

The vertical wind velocity component $\langle \overline{w} \rangle$ was obtained by averaging measurements from the 3-D sonic anemometers comprising the two eddy covariance stations. The local vertical advection $a_{v,2p}$ can be approximated as follows:

$$a_{v,2p} \;=\; \beta \cdot \langle \overline{w} \rangle \tag{18}$$

$a_{v,2p}$ is a constant, so integration over the height $\Delta z$ of the system and conversion to energetic units yields the total vertical advection:

$$A_{v,2p}(t) \;=\; c_H \cdot a_v \cdot \Delta z \;=\; c_H \cdot \beta \cdot \langle \overline{w} \rangle \cdot \Delta z \tag{19}$$

*Spatial Averaging Method (Lee, 1998):* Vertical advection was computed using a spatial averaging method according to the methods outlined by Lee (1998). The following equation was used to compute the vertical advection $A_{v,SA}$, which is a spatial average of the gradients corresponding to all station pairs including the top station.

$$A_{v,SA}(t) \;=\; c_H \cdot \overline{w}_{top} \cdot \left[ \overline{T}_{top} - \langle \overline{T} \rangle \right] \tag{20}$$

Here $\overline{w}_{top}$ and $\overline{T}_{top}$ represent the time-averaged vertical wind velocity component and temperature of the top station, respectively. $\overline{w}_{top}$ was obtained from the 3-D sonic anemometer corresponding to the top eddy covariance station.

### *3.3.4 Storage*

Storage is defined as the (partial) time derivative of the flow quantity of interest integrated over the control volume. The time derivative of temperature was approximated using the finite-difference method by computing central differences $\Delta T_i$ for the $i^{th}$ profile layer corresponding to each time interval $\Delta t$; i.e., $\left(\frac{\partial T}{\partial t}\right)_i \approx \left(\frac{\Delta T}{\Delta t}\right)_i$ (local storage). Therefore, the storage integral in Equation 10 becomes a sum:

$$S(t) \;=\; c_H \sum_i \left( \frac{\Delta T}{\Delta t} \right)_i \cdot \Delta z_i \tag{21}$$

### 3.3.5 Soil Heat Flux

A variety of methods exist which can be used to calculate the soil heat flux, as elucidated by Liebethal and Foken (2006). The most accurate method to date other than the conventional profile integration method (integration of temperature gradients over a logarithmic profile) is the force-restore method, which describes heat diffusion as a combination of a forcing function (i.e., heating due to solar radiation) and restorative cooling between the surface layer and a given sublayer. The force-restore method is often preferred over the profile integration method because it is only necessary to measure temperature at two depths for an accurate determination of the soil heat flux. Two approaches to the force-restore method are introduced in Blackadar (1976) Bhumralkar (1975). We chose to utilize the method corresponding to Bhumralkar (1975) because it was most consistent with the profile integration method. The equation outlined in Bhumralkar (1975) is as follows:

$$G(t) \;=\; \Delta z \cdot c_v \cdot \frac{\partial T_1}{\partial t} \;+\; \sqrt{\frac{\omega \cdot c_v \cdot \kappa}{2}} \cdot \left( \frac{1}{\omega} \frac{\partial T_1}{\partial t} \;+\; T_1 \;-\; \overline{T_2} \right) \tag{22}$$

Here $\Delta z$ is the absolute difference of the surface and base depths (the thickness of the "thermally active" soil layer), $T_1$ and $T_2$ are the temperatures corresponding to the surface and base depths (respectively), $c_v$ is the volumetric heat capacity of the soil, $\kappa$ is the soil thermal conductivity, and $\omega$ is the frequency corresponding to a 24-hour period (i.e., $\omega = 2\pi/86,400s^{-1}$). The overbar on $T_2$ represents a time average over the entire time series. In the present study, $T_1$ corresponded to a depth of 2 cm and $T_2$ corresponded to a depth of 8 cm. As with computation of the storage term, derivatives were approximated using the finite-difference method.

### 3.3.6 Residual

The residual of the energy budget was computed by subtracting the total energy budget (the sum of all energy budget components, including soil heat flux and latent vertical turbulent flux) from the net radiation. The residual is thus defined mathematically as follows:

$$R = -(R_N + Q_{v,H} + Q_{v,\lambda E} + A_h + A_v + S + G) \tag{23}$$

The residual was computed utilizing both methods for computing advection (i.e., linear approximation and spatial averaging). The residual was also computed excluding advection. The magnitude of the residual was compared to determine which method resulted in the highest degree of closure. The method of greatest closure (smallest residual) was used for conditional analysis, outlined in the following section.

## 3.4 Variability and Conditional Analysis

The relative influence of each energy budget component is likely to vary across space and time, as well as under varying conditions. The methods by which the variability of wind-temperature structure and the conditionally-defined influence of each energy budget component (particularly advection) are described in detail here. The following methods form the core of the study, for very little research on variability and conditional analysis has been done in comparison to mean climatalogical studies on the surface energy budget.

### *3.4.1 Variability*

The spatial variability of both temperature and wind velocity over the horizontal domain can be analyzed in a variety of ways. One approach is simply the visualization of wind and temperature fields and profiles, which can be obtained via spatial interpolation of wind and temperature measurements corresponding to the horizontal array and vertical profile station networks at various points in time. Such visual tools are very useful for gaining an intuitive understanding of variability of wind and temperature over space and time. However, a quantitative description of variability is also necessary. Using methods analogous to Mahrt et al (2009) and Thomas et al (2008), we defined the horizontal variability $\tilde{\rho}$ of a varying quantity as the difference between $\rho_i$ (the quantity $\rho$ corresponding to the $i^{th}$ station) and the horizontal network average $\langle\rho\rangle$:

$$\tilde{\rho} \ = \ \rho_i \ - \langle\rho\rangle \tag{24}$$

The variability of temperature, $T_{VAR}$, was defined as the absolute value of $\tilde{T}$:

$$T_{VAR} \ = \ |\tilde{T}| \tag{25}$$

Correspondingly, the variability of horizontal windspeed, $V_{VAR}$, was defined as the magnitude of the vector $(\tilde{u} \;\; \tilde{v})$:

$$V_{VAR} \;=\; \sqrt{\tilde{u}^2 + \tilde{v}^2} \tag{26}$$

Computing horizontal variability serves as a useful tool for evaluating the accuracy of the assumption of horizontal homogeneity.

#### *3.4.2 Conditional Analysis*

Energy transfer is a complex phenomenon. The influence of the various modes of energy transfer (e.g., turbulence and advection) not only vary over space and time, but also depend strongly on physical conditions. We sought to evaluate the physical conditions under which advection has the greatest influence on the energy balance, particularly in the context of turbulence kinetic energy (TKE, $k$) and the standard deviation of vertical wind speed ($\sigma_w$). TKE is defined as the fluctuating component of the time-averaged specific kinetic energy $\overline{e}_k = \frac{1}{2}\overline{\mathbf{v}\cdot\mathbf{v}}$ (obtained via Reynolds' Second Postulate):

$$k \;=\; \frac{1}{2}\cdot\left(\overline{u'u'} + \overline{v'v'} + \overline{w'w'}\right) \;=\; \frac{1}{2}\cdot\left(\sigma_u^2 + \sigma_v^2 + \sigma_w^2\right) \tag{27}$$

By plotting advection as a function of TKE and $\sigma_w$, we were able to determine how advection varies with increasing or decreasing turbulence strength. The results of the conditional analysis are directly relevant to our investigation of scalar similarity between sensible heat advection and advective carbon loss.

### 3.5 Scalar Similarity

Carbon fluxes obtained from the eddy covariance stations and subcanopy respiration data from Thomas et al (2013) were used to determine the degree of advective carbon loss. The advective carbon loss ($R_{SUB}$) was defined as the difference between NEE according to Thomas et al (2013) and Thomas et al (2008) and the traditional definition of NEE (i.e., $R_{SUB} \equiv NEE_{Thomas,2013} - NEE_{Trad.}$). The conventional method for calculating NEE includes only storage and the vertical turbulent carbon dioxide flux ($FCO_2$) measured in or above the canopy, while NEE according to Thomas et al (2013) and Thomas et al (2008) includes the effects of advective carbon loss, the fraction of total NEE which is hypothetically advected out of the control volume before reaching the canopy sensors under conditions when the above-canopy layer is

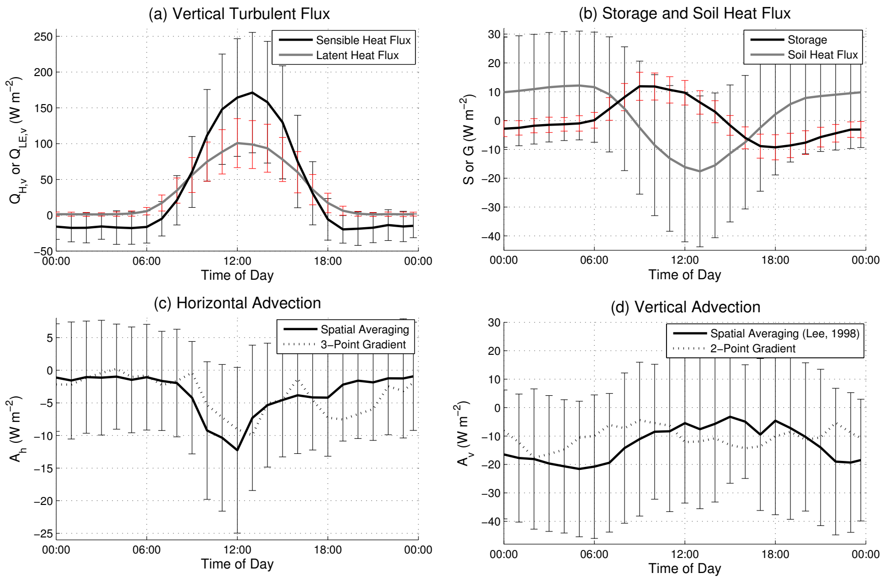


**Fig. 2** Ensemble mean diurnal course corresponding to period 27 August 2008 - 31 December 2009 of all calculated energy budget components (error bars span one standard deviation): (a) sensible and latent vertical turbulent fluxes, (b) storage and soil heat flux, (c) horizontal advection, and (d) vertical advection. Significant variation among the relative influence of budget components on total budget is evident. The vertical turbulent fluxes are much greater in magnitude than advective fluxes, storage, and soil heat flux during the day, but are on the same order of magnitude at nighttime.

decoupled from the subcanopy and ground surface layers. As elucidated in Thomas et al (2013) and Thomas et al (2008), neglecting the effects of advective carbon loss and decoupling will potentially lead to underestimations in NEE.

The absolute degree of advective carbon loss $|R_{SUB}|$ was plotted as a function of the absolute horizontal and vertical sensible heat advection $|A|$ to determine whether a clear relationship between sensible heat advection and advective carbon loss exists. $|A|$ was also plotted as a function of $|R_{SUB}|$ under strong advection and weak advection conditions determined from the conditional analysis.

## 4 Results and Discussion

### 4.1 Mean Climatology of Energy Flux Components

Results demonstrate varying influence of energy budget components on total energy budget and residual across time on both a diurnal and seasonal basis. Figure 2 shows the ensemble mean diurnal course of each energy budget component corresponding to the period 27 August 2008 - 31 December 2009 of all calculated energy budget

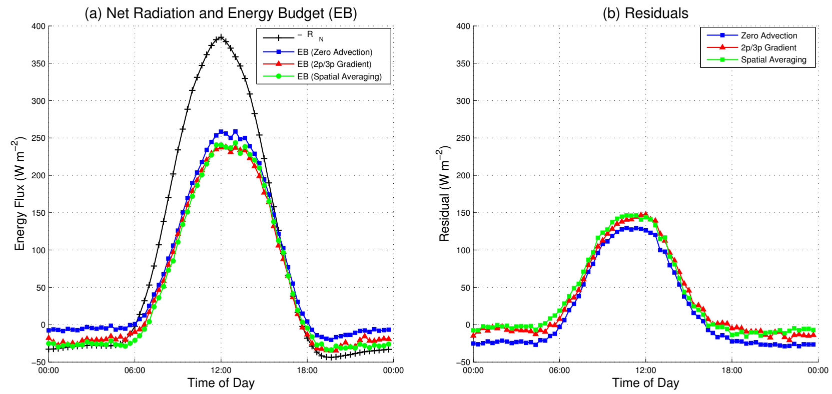


**Fig. 3** Ensemble mean diurnal course corresponding to period 27 August 2008 - 31 December 2009 of (a) total energy budget and (b) residual with and without advection, both calculation options (spatial averaging and linear approximation) included. Net radiation is included in plot (a) for comparison. Daytime residuals appear to be quite large (maximum $+150\ W\ m^{-2}$). Nighttime residual is significantly reduced (nearly zero) when advection is included using the spatial averaging method.

components. Error bars span one standard deviation. Both calculation options for computing advection (spatial averaging and linear approximation) are included for horizontal and vertical advection. It is clear the vertical turbulent sensible and latent heat fluxes have a much greater influence on the total energy budget than storage, advection, and the soil heat flux during the day, but such effects are drastically reduced at nighttime when all budget components are on a similar order of magnitude. Such results suggest that advection potentially plays a significant role in energy transfer at nighttime. In addition, both horizontal and vertical advection are negative, indicating that total advection is non-zero on average. Such results are evidence against the common assumption that horizontal and vertical advection ”balance out” to zero.

Figure 3 (a) shows the total energy budget ($Q_H + Q_{\lambda E} + A_H + A_V + S + G$) with and without advection (both calculation options included) in relation to the net radiation ($-R_N$). The corresponding residuals, defined by Equation 23, are also shown in Figure 3 (b). All residuals appear to be quite large during the day, with a maximum of $\sim 150\ W\ m^{-2}$ around midday. Further experimentation is necessary to determine the causes of such large daytime residuals. When advection is included in the energy budget, the magnitude of the daytime residual is larger than when zero advection is assumed. However, including advection clearly improves energy balance closure at nighttime by significantly reducing the residual from a relatively constant value of $-25\ W\ m^{-2}$ to nearly zero (especially between 00:00 and 06:00), providing additional evidence that advection plays an important role in energy transfer at nighttime.

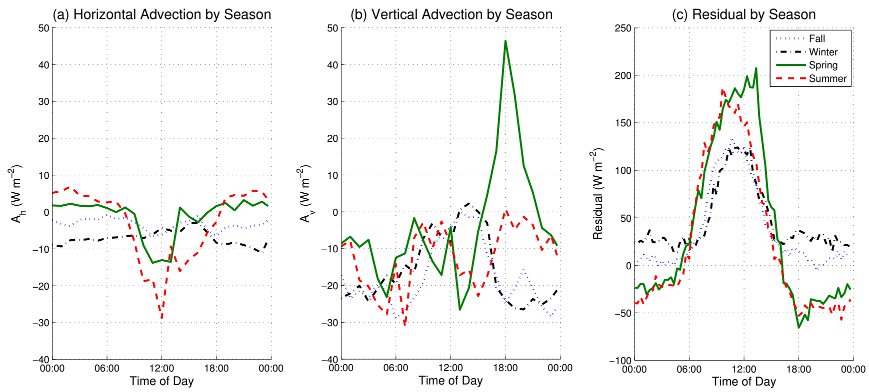


**Fig. 4** Ensemble mean diurnal course of (a) horizontal advection, (b) vertical advection, and (c) residual by season. The magnitude of horizontal advection is largest during the summer around midday (12:00). Vertical advection is particularly large and positive ($+45\ W\ m^{-2}$) in spring evenings (18:00) in comparison to other seasons and times of the day, where advection in all directions is mostly negative and varies between 0 and $-30\ W\ m^{-2}$; potentially the result of seasonal outliers. The nighttime residual tends to be at a maximum ($+40\ W\ m^{-2}$) during winter and at a minimum ($-50\ W\ m^{-2}$) during summer due to systematic seasonal underestimations and overestimations of the nighttime energy budget. However, if we recall the results of Figure 3 (b), it is clear that including advection in the total energy budget reduces the degree of such underestimation and overestimation so that the nighttime residual averages out to $0\ W\ m^{-2}$.

Although there is there is only a slight difference between the residuals corresponding to the spatial averaging and linear approximation methods for computing advection, the spatial averaging method leads to a higher degree of nighttime closure. This observation suggests that the assumption of uniform gradients is not valid within heterogeneous terrain. We will use the results corresponding to the spatial averaging method in all future figures and results.

Figure 4 shows the ensemble mean diurnal course corresponding to the period 27 August 2008 - 31 December 2009 of (a) horizontal advection, (b) vertical advection, and (c) residual by season using the spatial averaging method. Vertical advection is particularly large and positive ($+45\ W\ m^{-2}$) in spring evenings (18:00) in comparison to other seasons and times of the day, where advection in all directions is mostly negative and varies between 0 and $-30\ W\ m^{-2}$. Such a large value of advection may be unphysical and is potentially the result of seasonal outliers which were missed in the despiking process, although further experimentation is necessary to confirm this statement. The nighttime residual tends to be at a maximum ($+40\ W\ m^{-2}$) during winter and at a minimum ($-50\ W\ m^{-2}$). However, if we recall the results of Figure 3 (b), it is clear that including advection improves energy balance closure at nighttime. In essence, Figure 4 reveals that advection does not close the energy budget consistently at all times of the year, but instead reduces the degree of underestima-

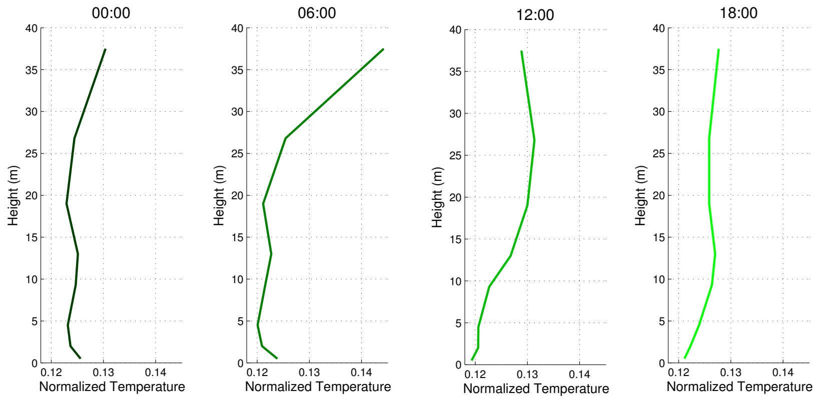


**Fig. 5** Linearly interpolated vertical temperature profile at 00:00, 06:00, 12:00, and 18:00, ensemble averaged over period 27 August 2008 - 31 December 2009. Dry-bulb temperature measurements were normalized with respect to the sum of all profile measurements at a given time, and therefore measurements in the above figure are unitless. Dry-bulb temperature was assumed to be approximately equal to potential temperature due to the minimal influence of buoyancy and hydrostatic effects within the spatial scale (height) of the profile.

tion or overestimation which occurs systematically from season to season so that the nighttime residuals average out to 0 $W\ m^{-2}$.

## 4.2 Spatial Variability

The most common simplifying assumptions with regard to spatial variability is that of horizontal homogeneity (zero advection) or spatially uniform gradients. Figure 5 shows the linearly interpolated vertical temperature profile (ensemble averaged over the period 27 August 2008 - 31 December 2009) at 00:00, 06:00, 12:00, and 18:00; dry-bulb temperature measurements were normalized with respect to the sum of all profile measurements at a given time, and therefore the temperature measurements in Figure 5 are unitless. Although potential temperature is a more desirable parameter for analyzing vertical temperature variability, we are assuming dry-bulb temperature is approximately equal to potential temperature due to the fact that buoyancy and hydrostatic effects have minimal influence within the height scale of our system. Figure 6 shows the inverse-square interpolated wind and temperature fields (ensemble averaged over the period 27 August 2008 - 31 December 2009) at 00:00, 06:00, 12:00, and 18:00.

It is evident from Figures 5 and 6 that variability exists in all directions, alluding to the inadequate nature of the assumption of homogeneity and uniform gradients. Significant nonlinear variability is present in Figure 6, particularly with respect

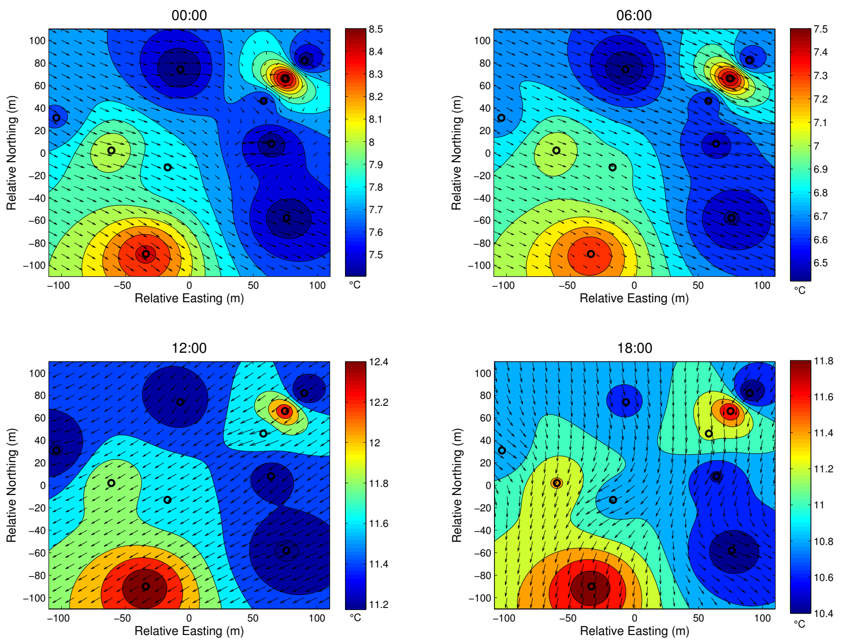


**Fig. 6** Inverse-square interpolated horizontal wind and dry-bulb temperature fields at 00:00, 06:00, 12:00, and 18:00, ensemble averaged over period 27 August 2008 - 31 December 2009. Spatial variability is most likely due to variation in both terrain and topography, confirming that horizontal homogeneity cannot be assumed in heterogeneous landscapes.

to temperature. Temperature gradients are relatively large along the SW-NE axis at all times and wind direction generally shifts from SE to SW between morning and evening. A higher degree of variability of horizontal wind direction is evident at 00:00 and 18:00 compared to 06:00 and 12:00. Such spatial variability of both temperature and wind is likely the result of variation in both topography and terrain. Nonlinear variability is also evident in the vertical direction, as is evidenced by the temperature profiles comprising Figure 5.

A more quantitative treatment of horizontal variability is made in Figure 7 , which shows the relative abundance of the horizontal wind and temperature variability ($T_{VAR}$ and $V_{VAR}$, defined by Equations 25 and 26) corresponding to each station, separated by day and night. Stations S05, S06, and S08 have the highest mean value of $T_{VAR}$ and Stations S05, S09, and S10 have the highest mean value of $V_{VAR}$, but temperature and wind speed variability is present in all stations and varies noticeably from station to station. The spread of the distributions of both $T_{VAR}$ and $V_{VAR}$ tend to be slightly larger during the day, implying a higher degree of variability during daytime than at nighttime. The fact that the mean values of $T_{VAR}$ and $V_{VAR}$ are greater than zero

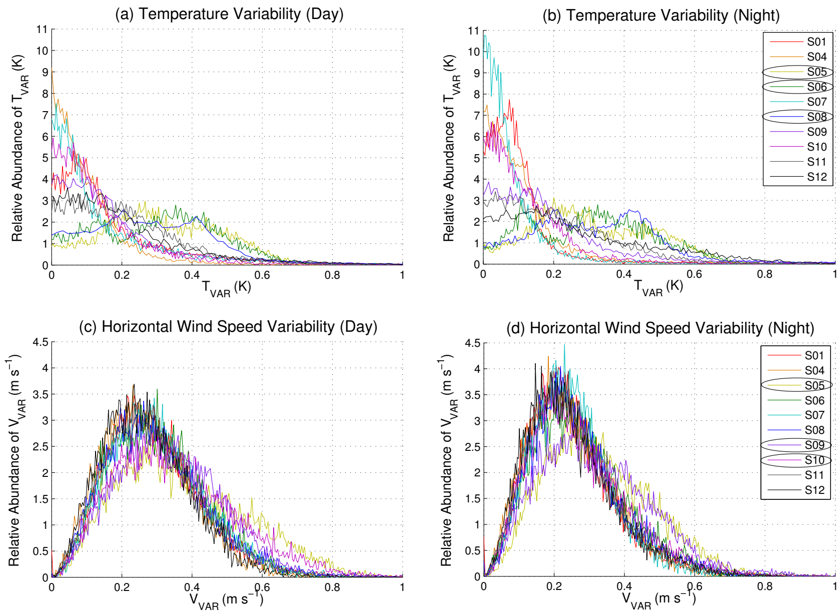


**Fig. 7** Relative abundance of of $T_{VAR}$ and $V_{VAR}$ corresponding to each station, separated by day and night. Stations S05, S06, and S08 have the highest mean value of $T_{VAR}$ and Stations S05, S09, and S10 have the highest mean value of $V_{VAR}$, but temperature and wind speed variability is present in all stations and varies noticeably from station to station. The spread of the distributions of both $T_{VAR}$ and $V_{VAR}$ tend to be slightly larger during the day, implying a higher degree of variability during daytime than at nighttime. Such results are quantitative evidence of horizontal spatial variability which was apparent in Figure 6.

and variation of the mean values of $T_{VAR}$ and $V_{VAR}$ from station to station exists provides a quantitative confirmation of the inadequacy of the assumptions of horizontal homogeneity and uniform gradients.

## 4.3 Conditional Analysis

Figure 8 shows the median-binned plots of horizontal and vertical advection as a function of TKE and $\sigma_w$ corresponding to both the above-canopy and subcanopy eddy covariance stations. Error bars span one median absolute deviation. Figure 8 (a) includes normalized probability distribution functions (multiplied by a factor of 10) of the absolute value of horizontal and vertical advection, which were used to determine physical criteria for strong and weak advection. All plots in Figure 8 demonstrate a similar trend, allowing us to draw a relationship between turbulence strength (TKE or $\sigma_w$) and advection: as turbulence strength increases from zero, the magnitude of advection (horizontal or vertical) approaches a maximum value and then decreases

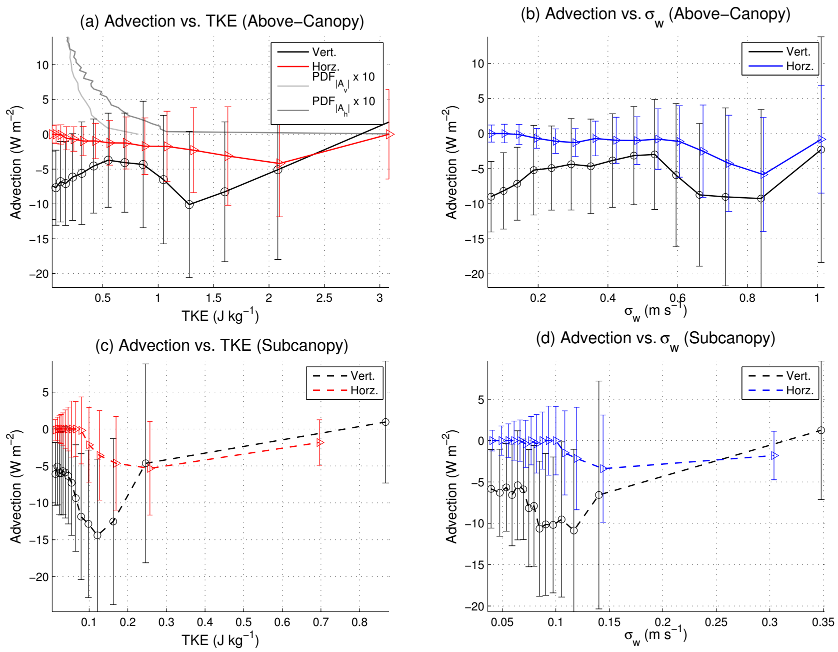


**Fig. 8** Median-binned plots of horizontal and vertical advection as a function of TKE and $\sigma_w$ corresponding to both the above-canopy and subcanopy eddy covariance stations. Error bars span one median absolute deviation. Plot (a) includes normalized probability distribution functions (multiplied by a factor of 10) of the absolute value of horizontal and vertical advection, which were used to determine physical criteria for strong and weak advection. All plots demonstrate that advection is strongest at intermediate values of turbulence strength (TKE or $\sigma_w$). For example, the magnitude of vertical advection is maximal ($-15\ W\ m^{-2}$) when subcanopy TKE is close to $0.1\ J\ kg^{-1}$ and the magnitude of horizontal advection is maximal ($-5\ W\ m^{-2}$) when subcanopy TKE is close to $0.25\ J\ kg^{-1}$. The magnitude of both vertical and horizontal subcanopy advection become small when TKE becomes very small or very large.

toward zero when turbulence becomes strong. In other words, advection tends to be strongest at intermediate values of turbulence strength (TKE or $\sigma_w$). This trend is especially clear in Figure 8 (c), where the magnitude of vertical advection is maximal ($-15\ W\ m^{-2}$) when subcanopy TKE is approximately $0.1\ J\ kg^{-1}$ and the magnitude of horizontal advection is maximal ($-5\ W\ m^{-2}$) when subcanopy TKE is close to $0.25\ J\ kg^{-1}$. As subcanopy TKE becomes either very small or very large, both horizontal and vertical advection become very small. In combination with Table 1, Figure 8 provides clear evidence that advection is strongest at intermediate values of TKE and $\sigma_w$. Separating strong and weak advection is an important step in evaluating scalar similarity between sensible heat advection and advective carbon loss, the results of which are discussed in the following section.

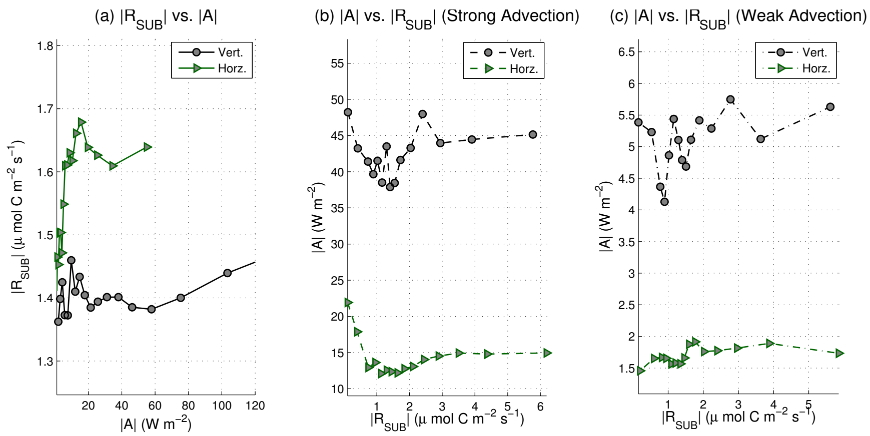


**Fig. 9** Median-binned plots of (a) advective carbon loss ($R_{SUB}$) as a function of sensible heat advection ($A$), (b) strong sensible heat advection as a function of advective carbon loss, and (c) weak sensible heat advection as a function of advective carbon loss. Horizontal and vertical advection are plotted separately, and all quantities are absolute. It is clear from plot (a) that $|R_{SUB}|$ increases with $|A|$ in a nonlinear fashion, particularly with respect to horizontal advection. In terms of plots (b) and (c), a relatively smooth nonlinear correlation between advection and $|R_{SUB}|$ is apparent under strong advection conditions, while such a relationship is not clear under weak advection conditions. Under strong advection conditions, advection tends to be largest when $|R_{SUB}|$ is zero. As $|R_{SUB}|$ increases, advection tends to decrease in magnitude and reach a minimum, followed by an increase toward a constant value as $|R_{SUB}|$ becomes large.

## 4.4 Scalar Similarity

Figure 9 shows the median-binned plots of (a) advective carbon loss ($R_{SUB}$) as a function of sensible heat advection ($A$), (b) strong sensible heat advection as a function of advective carbon loss, and (c) weak sensible heat advection as a function of advective carbon loss. Horizontal and vertical advection are plotted separately. All quantities are plotted in terms of absolute value. Conditions of strong and weak advection were defined quantitatively as any measurement above or below the 50th percentile of the distribution function (respectively) of absolute advection. The criteria for for separating strong and weak advection were applied to determine if a clear relationship exists between sensible heat advection and advective carbon loss under such conditions. It is clear from Figure 9 (a) that $|R_{SUB}|$ increases with $|A|$ in an apparently nonlinear fashion, particularly with respect to horizontal advection. Although further experimentation is necessary to precisely examine this relationship, it is clear that the degree of advective carbon loss increases with increasing sensible heat advection, especially in the horizontal domain.

In terms of Figure 9 (b) and Figure 9 (c), there is a relatively smooth nonlinear correlation between sensible heat advection and $|R_{SUB}|$ under strong advection conditions, while such a relationship is not clear under weak advection conditions. Under strong advection conditions, advection tends to be largest when $|R_{SUB}|$ is zero. As $|R_{SUB}|$ increases, advection tends to decrease in magnitude and reach a minimum, followed by an increase toward a constant value as $|R_{SUB}|$ becomes large. This relationship is most clear with respect to horizontal advection, in which the curve is quite smooth. As $|R_{SUB}|$ increases from zero, the magnitude of horizontal advection under strong advection conditions decreases and reaches a minimum value of $\sim 12\ W\ m^{-2}$ and approaches $\sim 15\ W\ m^{-2}$ asymptotically as $|R_{SUB}|$ becomes large. The results of Figure 9 (b) and Figure 9 (c) have interesting implications, as they demonstrate that $|R_{SUB}|$ is most tightly correlated with strong, horizontal advection. However, the apparent correlation between strong advection and $|R_{SUB}|$ exists primarily when $|R_{SUB}|$ is small, as advection approaches a constant when $|R_{SUB}|$ becomes large.

## 5 Conclusions

The overarching goals of the present study were to investigate the role of sensible heat advection in the surface energy balance and under various physical conditions, evaluate the validity of the assumption of horizontal homogeneity and uniform gradients in heterogeneous landscape via analysis of spatial variability of wind and temperature, and explore scalar similarity between sensible heat advection and advective carbon loss to determine whether heat advection may be used as a predictor of carbon loss due to decoupling. The results from Section 4 have led us to the following conclusions:

1. Sensible heat advection plays a significant role in energy balance closure at nighttime when turbulent fluxes are small.
2. In general, total advection is non-zero (advective fluxes do not balance out).
3. It is invalid to assume horizontal homogeneity and uniform gradients in heterogeneous terrain.
4. Advection tends to be strongest at intermediate values of turbulence strength (TKE or $\sigma_w$) and approaches zero as turbulence strength becomes very small or very large.
5. There is a potential nonlinear relationship between sensible heat advection and advective carbon loss in the subcanopy. The degree of advective carbon loss is most tightly correlated with strong, horizontal advection.

Conclusion (1) confirms that advection has an influence on the energy balance. Conclusions (2) and (3) confirm that simplifying physical assumptions should not be assumed when computing energy fluxes, as stringent constraints such as horizontal homogeneity, uniform gradients and zero advection are not physically valid in heterogeneous terrain. Conclusion (4) can be explained by the fact that wind speed tends to increase with turbulence strength. If we recall that advection is the product of wind speed and temperature gradient, we should expect advection to be zero when turbulence strength and wind speed are zero; we should also expect advection to be zero when turbulence strength and wind speed are high because the temperature gradient approaches zero as wind speed becomes large. Therefore, intermediate turbulence strength is where we should expect to observe strong advection. Conclusion (5) provides potentially interesting implications for ecologists and atmospheric scientists alike. If a functional relationship exists between sensible heat advection and advective carbon loss, it will be possible to analyze the dynamics of a complex biological process (carbon transfer) using purely physical variables. As indicated by the present study, such a relationship is most likely to exist under strong advection conditions on the horizontal plane. Finding a precise relationship between strong, horizontal sensible heat advection and advective carbon loss will be an interesting and necessary topic of future studies.

## Acknowledgments

NSF Grant, AGS 0955444, DOE DE-FGO2-OGER64318

Dr. Christoph Thomas, Dr. Chad Higgins (Mentors)

Dr. Kate Field (Bioresource Research Director)

Wanda Crannell (Academic Advisor)

Susan and Steve Carrigg (Parents)

Bioresource Research Program and Oregon State University

## References

Anthoni PM, Law BE, Unsworth MH, Vong RJ (2000) Variation of Net Radiation over Heterogeneous Surfaces: Measurements and Simulation in a Juniper-Sagebrush Ecosystem. Ag and Forest Meteorol 102(4):275–286

Arya S (2001) Introduction to Micrometeorology, International Geophysics Series, vol 79, 2nd edn. Academic Press, San Diego, London

Aubinet M, Berbigier P, Bernhofer CH, Cescatti A, Feigenwinter C, Granier A, Grunwald TH, Havrankova K, Heinesch B, Longdoz B, Marcolla B, Montagnani L, Sedlak P (2005) Comaring co2 storage and advection conditions at night at different carboeuroflux sites. Bound Layer Meteorol 116(1):63–94

Aubinet M, Feigenwinter C, Heinesch B, Bernhofer C, Canepa E, Lindroth A, Montagnani L, Rebmann C, Sedlak P, van Gorsel E (2010) Direct advection measurements do not help solve the night-time co2 closure problem: Evidence from three different forests. Ag and Forest Meteorol 150(5):655–664

Bhumralkar CM (1975) Numerical experiments on the computation of ground surface temperature in an atmospheric general circulation model. J Appl Meteorol 14:1246–1258

Blackadar AK (1976) Modeling the nocturnal boundary layer. Preprints of the Third Symposium on Atmospheric Turbulence and Air Quality (Rayleigh, NC), Amer Meteorol Soc pp 46–49

Bowen IS (1926) The Ratio of Heat Losses by Conduction and by Evaporation from Any Water Surface. Physical Review 27:779–787

Feigenwinter C, Bernhofer C, Vogt R (2004) The Influence of Advection on the Short Term CO2 Budget In and Above a Forest Canopy. Bound Layer Meteorol pp 201–224

Finnigan J (1999) A Comment on the Paper by Lee (1998): "On Micrometeorological Observations of Surface-Air Exchange over Tall Vegetation". Ag and Forest Meteorol 97(1):55–64

Foken T (2008a) Micrometeorology. Springer, Berlin, Heidelberg

Foken T (2008b) The Energy Balance Closure Problem: An Overview. Ecologic Appl 18(6):1351–1367

Foken T, Wimmer F, Mauder M, Thomas C, Liebethal C (2006) Some aspects of the energy balance closure problem. Atmos Chem Phys 6:4395–4402

Halldin S, Lindroth A (1992) Errors in Net Radiometry - Comparison and Evaluation of 6 Radiometer Designs. J Atmos Ocean Technol 9(6):762–783

Lee X (1998) On Micrometeorological Observations of Surface-Air Exchange Over Tall Vegetation. Ag and Forest Meteorol 91(1-2):39–49

Leuning R, Van Gorsel E, Massman WJ, Isaac PR (2012) Reflections on the Surface Energy Imbalance Problem. Ag and Forest Meteorol 156:65–74

Liebethal C, Foken T (2006) Evaluation of Six Parameterization Approaches for the Ground Heat Flux. Theor and App Climatol 88(1-2):43–56

Mahrt L, Thomas CK, Prueger JH (2009) Space-time structure of mesoscale motions in the stable boundary layer. Q J R Meteorol Soc 135:67–75

Moderow U, Feigenwinter C, Bernhofer C (2007) Estimating the Components of the Sensible Heat Budget of a Tall Forest Canopy in Complex Terrain. Bound Layer Meteorol 123(1):99–120

Moderow U, Aubinet M, Feigenwinter C, Kolle O, Lindroth a, Molder M, Montagnani L, Rebmann C, Bernhofer C (2009) Available Energy and Energy Balance Closure at Four Coniferous Forest Sites across Europe. Theor and App Climatol 98(3-4):397–412

Stull RB (1988) An Introduction to Boundary Layer Meteorology. Atmospheric Sciences Library, Kluwer Acad. Publ., Dordrecht, Boston, London

Thomas CK (2011) Variability of Sub-Canopy Flow, Temperature, and Horizontal Advection in Moderately Complex Terrain. Bound Layer Meteorol 139(1):61–81

Thomas CK, Martin JG, Goeckede M, Siqueira MB, Foken T, Law BE, Loescher HW, Katul G (2008) Estimating Daytime Subcanopy Respiration from Conditional Sampling Methods Applied to Multi-Scalar High Frequency Turbulence Time Series. Ag and Forest Meteorol 148(8-9):1210–1229

Thomas CK, Martin JG, Law BE, Davis K (2013) Toward Biologically Meaningful Net Carbon Exchange Estimates for Tall, Dense Canopies : Multi-Level Eddy Covariance Observations and Canopy Coupling Regimes in a Mature Douglas-Fir Forest in Oregon. Ag and Forest Meteorol 173:14–27

Vickers D, Thomas C, Law BE (2009) Random and systematic co2 flux sampling errors for tower measurements over forests in the convective boundary layer. Ag and Forest Meteorol 149:73–83

Vogt S, Thomas P (1995) Sodar - a Useful Remote Sounder to Measure Wind and Turbulence. J Wind Eng Ind Aerodyn 54:163–172

Whiteman CD, Hubbe JM, Shaw WJ (2000) Evaluation of an inexpensive temperature datalogger for meteorological applications. J Atmos Ocean Technol 17(1):77–81